Effects of different fluids on microcrack propagation in sandstone under true triaxial loading conditions

Shaobin Hu (iD), Tunnel and Underground Engineering Institute, College of Civil and Transportation Engineering, HoHai University, JiangSu, NanJing, China
Xiaochun Li and Bing Bai, Institute of Rock and Soil Mechanics, Chinese Academy of Sciences, State Key Laboratory of Geomechanics and Geotechnical Engineering, Wuhan, Hubei, China

Abstract: The mechanical behavior of rock under conditions of multiphase fluids is currently a key scientific issue in the field of geotechnical engineering. In this work, we conducted triaxial compression experiments of initially water-saturated samples, which were flooded with CO_2 using the semipermeable separator method; comparatively investigated the mechanical behaviors of sandstone under the conditions of mono-phase fluids CO_2/N_2/H_2O and biphase fluid CO_2-H_2O; and analyzed the stress-strain characteristics, internal crack expansion, and macrocrack failure patterns of sandstones. Compared with H_2O, CO_2 and N_2 could lead sandstone cracks to show a pattern of multiple fractures, displaying a double shear failure mode and multiple branch cracks along principal fractures. Moreover, the cracking effect of supercritical CO_2 was more evident. Under the conditions of pore pressure of 10 MPa and temperature of 323 K, the ratio of work done by CO_2, N_2 and H_2O during crack expansion was 23.5:24.1:1, with transient pressure drops to 7.82 MPa, 9.25 MPa, and 0.1 MPa, respectively. Overall, the study analyzed the mechanisms of physicochemical interactions of fluid types and the number of phases in sandstone minerals at the microscale and revealed the mechanical mechanism between fluids and rock minerals, as well as the impacts of these fluids on the strength, internal crack expansion and deformation of sandstone. © 2017 Society of Chemical Industry and John Wiley & Sons, Ltd.

Keywords: CO_2-H_2O biphase fluid; microcracking mechanism; failure pattern; triaxial test

Introduction

With the development of rock mechanics engineering, a growing number of cases are being related to pore fluid conditions. Research studies on the action of rock mechanics with pore fluid are gradually becoming problems of interest in the field of geotechnical engineering. The injection of artificial fluid into deep strata changes the pore pressure and fluid components and may lead to surface uplift, caprock rupture,[1,2] and fault activation and induce earthquakes.[3,4] For example, In Salah CO_2 geological sequestration project, the surface bulged upward at an average rate of 5 mm per year, causing the project to be halted temporarily.[4] Keith et al.[5] found that the greater injection pressure of the fluid, the greater the injection volume; and the faster the injection rate, the higher the risk of caprock rupture and fault reactivation.

With the implementation of underground geotechnical engineering projects such as CO_2

geological sequestration, geothermal development, and hydraulic fracturing, researchers have realized that underground fluid can significantly impact rock strength, deformation, and crack expansion. Many scholars have conducted triaxial experiments to study the coupled behavior of fluid (e.g. CO_2, CH_4, N_2, He, water, brine) migration during mechanical testing with various rock types (e.g. sandstone, mudstone, coal) and to examine their flow and strength behaviors.[6–9] Younane *et al.*[10] designed an inclined direct shear testing device and investigated the effects of pore fluid types on the strength of specimens. They found that the deformation and strength properties, i.e., cohesion and friction angle, can be highly sensitive to fluid composition and exposure time.[11–13] Moreover, physical and chemical actions can also greatly affect rock mechanical properties.[14] Grgic and Giraud[15] assumed that the pore mechanical and chemical effects of fluids at crack tips are responsible for the subcritical propagation of microcracks. Rostom *et al.*[16] used the double-torsion technique to measure the effect of fluid chemistry on the slow propagation of cracks in single crystals of calcite at room temperature and found that the chemical effect had a clear influence on crack propagation. Philip *et al.*[17] studied the damage and rupture processes of drying and water-saturated volcanic rocks and found that water lessened the strength of volcanic rocks and the propagation of interior cracks. Schoenball *et al.*[18] examined the microseismicity triggered by fluid injection and found that fluid injection worsened the instability of strata. Li Q *et al.*[19] used their acoustic emission system to monitor the failure mechanisms of sandstone and granite during CO_2 injection and found that CO_2 injection promoted the nucleation and propagation of cracks in rocks, leading to sudden rock destabilization. Niezgoda *et al.*[20] studied the thermodynamic behavior of carbon dioxide and confirmed its effectiveness as a medium for rock fracturing. Taoying Liu *et al.*[21] studied the opening and damage development characteristics of cracks subject to both compressional shear stress and porous fluids and proposed an equation for the evolution of the intensity factor of multiple rock cracks that combines the action of compression-shear stress and pore fluid pressure. It is well known that hydrous conditions strongly influence the mechanical behaviors of porous rocks. In summary, fluids act through two main mechanisms, namely, hydromechanical coupling and their chemical effects.

In fact, the effects of different pore fluids such as CO_2, CH_4, N_2, He, water and brine on a rock's strength, deformation, damage, and internal crack propagation have significant differences. However, real geological engineering projects often refer to the coupling of multiphase fluids; thus, different deformation and damage mechanisms induced by different fluids cause the mechanical problems to become more complicated in the rock. Yoshitaka *et al.*[22] used the load relaxation method of the Double Torsion (DT) testing method to measure both the crack velocity and the stress intensity factor under controlled temperature and relative humidity. More recently, Nara *et al.*[23–25] reported that the influence of the relative humidity on the crack velocity in rock was more significant when the rock is composed of larger amounts of clay minerals such as smectite and illite. Similarly, the injection of high-pressure artificial fluids into deep strata forms heterogeneous zones, inevitably resulting in the enhancement of the instability of the layered structure. Liteanu *et al.*[26] studied the effect of supercritical CO_2 displacing water on the strength of rock and found that the CO_2 dissolved into the water phase, leading to an acidic fluid that reduced the strength of the rock. Liu M *et al.*[27] adopted the semipermeable separator method to conduct their water displacement test under specific conditions of pressure and saturation, implemented the experiment with CO_2-H_2O biphase fluids fracturing a thick sandstone cylinder wall, and found that carbon dioxide has little effect on the tensile strength of sandstones. It is clear that the effects of single-phase fluids on rock strength and crack propagation have been studied more, and studies of rock mechanical behavior under the coupling of multiphase flow are lacking.

However, domestic and foreign research has shown that carbon dioxide is injected into the salt water layer and gradually dissolves in salt water, so that there are three kinds of fluid transition zones in specific layers, namely, the carbon dioxide concentration zone, mixed pressure zone and salt water area.[28] CO_2 and H_2O have very different thermophysical properties. Supercritical CO_2 has dual characteristics of both gas and liquid, namely, high density, low viscosity, and easy diffusion and compression. The mechanical behavior of the rock mass is highly dependent on the physical and chemical properties of the pore fluid, and there is a fluid interface in the CO_2-H_2O mixed phase, which complicates the process and mechanism of the interactions among CO_2, water, and rock mineral

|

particles. Clearly understanding the mechanical properties of rocks coupled with CO_2-H_2O biphase fluid is the key for evaluation of the mechanical stability of large-scale CO_2 geological sequestration. However, under the restraints of accurate control and measurement techniques of CO_2 and H_2O composition pressures and saturation degrees in the state of complex stresses, true triaxial mechanical experiments with rocks subject to CO_2-H_2O biphase fluids have been advancing quite slowly.

In addition, the role of CO_2 as a free pore fluid in rocks is commonly ignored. Similar to the phenomenon that the phase transition of deep water at high temperature accelerates fault slip and fracture,[29] the phase transition of CO_2 under the influence of high temperature, volume and pressure also impacts fault stability.[30] Further, the injection of CO_2 with high solubility into a deep formation leads to the production of CO_2-H_2O biphase fluids in strata pores. Therefore, modeling the stress and fluid states of deep reservoirs, implementing true triaxial mechanical comparative experiments with sandstone in the conditions of CO_2/N_2/H_2O fluids and CO_2-H_2O biphase fluid, and analyzing the stress-strain characteristics of sandstone, expansion of its interior cracks and failure modes of macroscopic cracks, as well as the impacts of these fluids on crack propagation, rock strength and deformation, are all significant for the risk assessment of the mechanical stability of large-scale CO_2 geosequestration sites.

Samples and experimental set-up

Samples

Homogeneous sandstone samples were selected for the experiments from Zigong, Sichuan Province, China. To eliminate or reduce the variability of rock mineral composition and pore structure or microcracks caused by spatial changes and deposition times, we carefully selected a homogeneous sample. Before performing fluid injection experiments, we conducted much experimental research on the mechanical properties of dry sandstone and found that, under the same conditions, the strength and mechanical behaviors of dry sandstone are very similar, with an error rate within 3%, which met our experimental requirements. The samples were polished into standard blocks with sizes of 50 mm × 50 mm × 100 mm to comply with the international standards of the Society of Rock

Mechanics and placed in a desiccator before use. Figure 1(a) shows the installation of samples.

According to the reference of GB/T 23561.2-2009,[31] the porosity was 8.77% measured by the liquid saturation method. The liquid permeability was measured at 0.042 mD based on the stable flow method under a confining pressure of 5 MPa and differential fluid pressure of 2 MPa between the two ends of the specimen. The crystallized mineral phases of sandstone were composed of 50.73% quartz, 34.01% albite, 10.59% calcite, 3.32% illite, and 1.36% montmorillonite as tested by X-ray diffraction experiments. Their mean pore diameter was 1350 nm as measured by the mercury intrusion method. Table 1 lists the compositions and contents of three samples.

Experimental set-up

Based on a true triaxial testing machine, we developed a suction control unit and established a two-phase flow coupled rock experimental system, as shown in Fig. 1(b).

The testing system was composed of three sub-modules: the triaxial stress control, pore fluid control and deformation measurement. The setup could separately and accurately control the triaxial stresses and the CO_2\$N_2$\$H_2O$ fluid pressure and precisely measure the transient qualities, flow rates and other parameters of CO_2 and H_2O. The triaxial loading was supplied by two rigid pads in the horizontal directions (loading axes I and II), and the hydraulic pressure in the vertical direction (loading axis III, e.g. confining pressure direction). The system was compatible with the samples with sizes of 50 mm × 50 mm × 100 mm and 40 mm × 40 mm × 80 mm.

The pore fluid pressure was accurately controlled and measured using a D series 100DX metering pump with constant pressure and constant flow rate operation modes (Teledyne ISCO, Lincoln, NE, USA). The constant pressure operation mode could provide a pressure in the range from 0.06895 MPa to 68.95 MPa at a display pressure resolution of 6.895 kPa. The Pcmax separator was a high air entry ceramic plate or a dense rock with a stable breakthrough pressure, which could effectively regulate and control the pore fluid pressures of CO_2 and H_2O by the axis-translation suction control technique. Figure 1(c) shows the true triaxial testing system for the biphase flow.

The instrument was composed of a temperature control subsystem, a triaxial loading subsystem, a
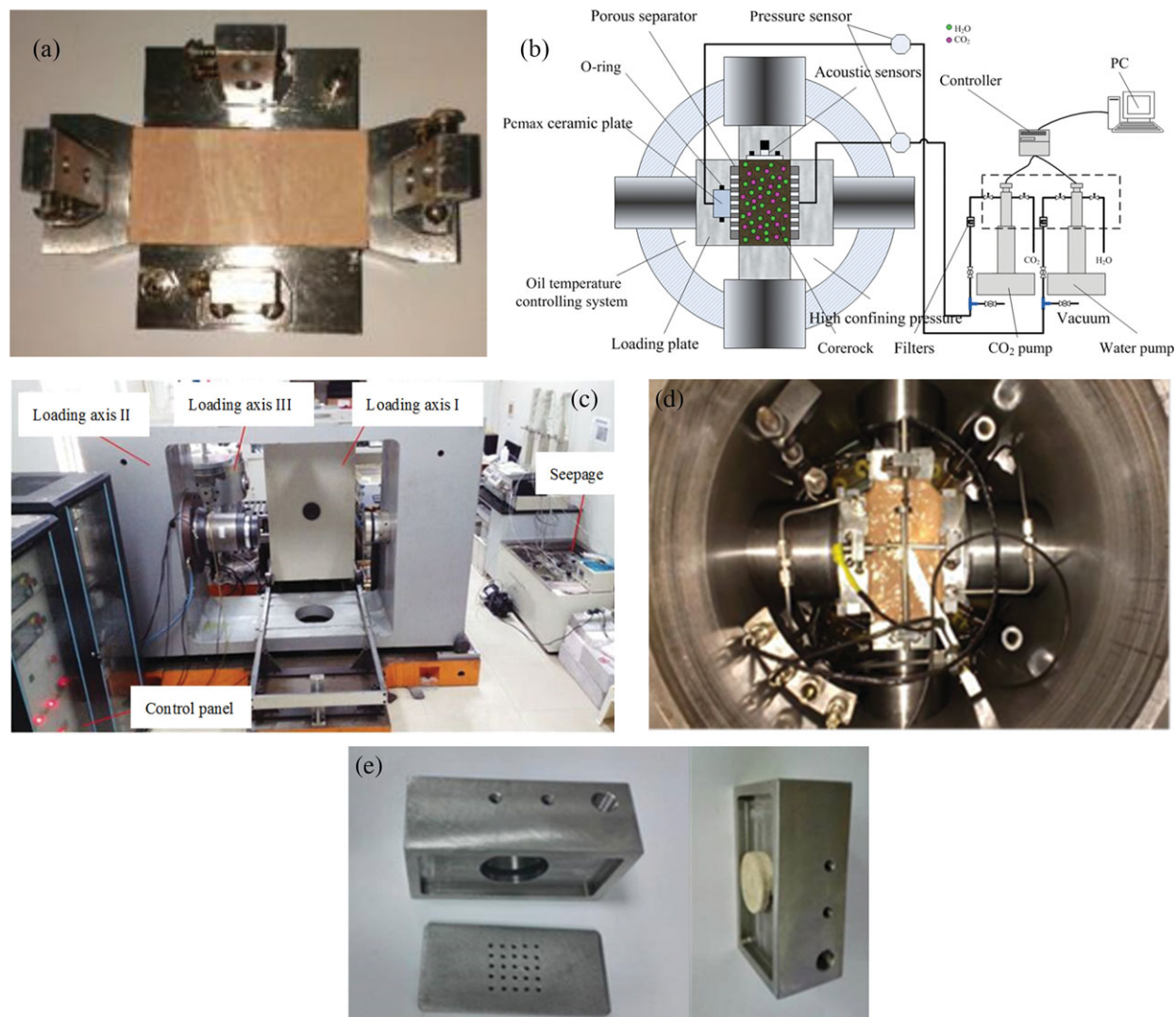
Figure 1. True Triaxial Experiment System: (a) a standard sample for the true triaxial mechanical test on sandstone; (b) schematic diagram of the true triaxial experimental system under two-phase flow conditions; (c) the true triaxial two-phase flow coupled rock testing system; (d) the triaxial pressure chamber with a sample loaded; (e) the triaxial loading plate for the CO_2-H_2O biphase fluid.

Table 1. Mineral composition of the sample.

Component	Quartz	Albite	Calcite	Illite	Montmorillonite
Content (%)	50.73	34.01	10.59	3.32	1.36

two-phase fluid control subsystem, and a data acquisition subsystem. The temperature control subsystem included a water bath and an external circulating water bath to control the temperatures of the pressure chamber and the ISCO pump, respectively, in the range of 10~95±0.1°C. The two-phase fluids control subsystem included two ISCO pumps and a semipermeable plate. The two ISCO pumps were used

to control the pore water and CO_2 pressure, and the plate was used to precisely control the CO_2 partial pressure and saturation. The entry pressure for the non-wetting phase of the plate was 1.5 MPa. When the differential pressure between the CO_2 in the specimen and the water in the plate was below 1.5 MPa, only water but not CO_2 could pass the plate. The data acquisition subsystem could record flow rate,

Table 2. Detailed parameters of contrast experiments.

Pore fluid	Pore fluid pressure/ MPa	Vacuum time/h	Fluid equilibration time/h	Temperature/ K	Stress 2/ MPa	Stress 3/ MPa	Load rate/ (/s)
None	0	6	12	323	15	10	1.0×10^{-5}
N_2	10	6	12	323	25	20	1.0×10^{-5}
CO_2	10	6	12	323	25	20	1.0×10^{-5}
H_2O	10	6	12	323	25	20	1.0×10^{-5}
CO_2-H_2O	CO_2/10+H_2O/8.5	6	12	323	25	20	1.0×10^{-5}

volume, and pressure data of the ISCO pumps in real time.

Experimental contents and procedure

Experimental contents

To determine the different effects of N_2, CO_2 and water on the mechanical properties of rocks, true triaxial tests of sandstone were conducted under the conditions of dry rock, N_2, CO_2, and water flow, and CO_2-H_2O two-phase flow. Based on the phase transition of supercritical CO_2 and the pore fluid state in the reservoir stratum, the experiments were conducted under a pressure of 10 MPa at 50°C. The detailed test parameters are listed in Table 2.

Based on the properties of the test fluids, two types of tests were conducted.

- Type 1: True triaxial tests of dry rock and rocks containing N_2, CO_2 and H_2O to determine the strength, stress, and strain of rocks with different single-phase pore fluids and to reveal the effective mechanisms of different pore fluids.
- Type 2: Tests with the CO_2-H_2O two-phase flow that accurately controlled the component pressures of CO_2 and H_2O to characterize the rock mechanical properties including strength under the influence of the two-phase flow and to determine its effective mechanism.

Experimental design and procedure

Figure 1(d) shows the triaxial pressure chamber with a sample loaded. The position of the sample was adjusted using a sample positioning device to facilitate the sample loading, avoid loading eccentricity, and thus ensure the accuracy of the true triaxial test. The gaps between the sample and the pad were sealed to isolate the sample from the hydraulic oil.

The pore fluid pressure and flow rate were accurately controlled and precisely measured with an ISCO metering pump. The constant pressure operation mode could provide a pressure in the range from 0.06895 MPa to 68.95 MPa at a display pressure resolution of 6.895 kPa. To control the component pressures of CO_2 and H_2O, suction control technology was added to the original design based on the experimental experience using unsaturated soil. Figure 1(e) shows the modified true triaxial loading pad based on the axis translational method.

The Type 2 experimental procedure included five stages: sample installation, pre-vacuum, pore water/gas saturation, flooding and loading.

1) The sample was mounted in the pressure chamber as shown in Fig. 1(d).
2) The pressure chamber was then pre-vacuumed and connected to the triaxial loading system, two-phase flow system and data acquisition system. The temperature of the hydraulic oil was increased to 323 K by the temperature control system. The confining pressure (sigma_2 = sigma_3) in the pressure chamber was increased to 20 MPa (10 MPa for dried sandstone). The system was then vacuumed for 6 h.
3) The vacuum pump was shut down, and the values were closed. The metering pumps for pore fluids (N_2\$CO_2$\$H_2O$) were set to the desired pore fluid pressures according to Table 2 in the constant pressure mode for 6 h to allow the sandstone to become saturated with the pore fluids.
4) The CO_2 pore pressure was increased to the desired value with the metering pump operated in the constant pressure mode. For CO_2 flooding, the first step was to open the valve to allow CO_2 into the specimen from the bottom to displace water in the specimen. With higher pressure of CO_2 in the pores of the specimen, pore water was compressed,
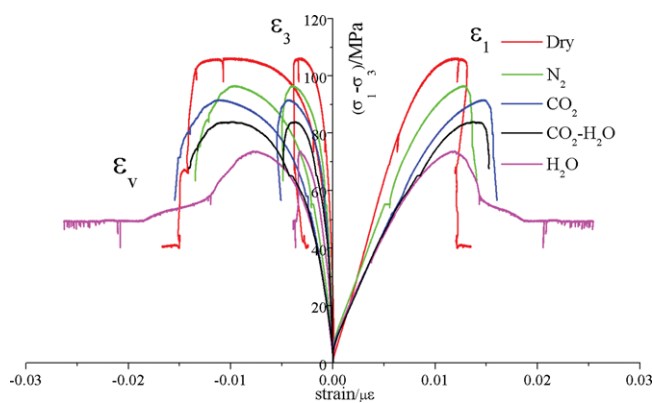
Figure 2. True triaxial mechanical tests with single phase pore fluids.

leading to an increase in pore water pressure. To keep pressure constant, the pore water pump in the constant pressure mode was in the fallback state, moving the pore fluid in the direction of the pump. As the pore water was driven out of the pores, CO_2 saturation in the specimen gradually increased. Consequently, CO_2 in the specimen moved to smaller pores to replace water. This replacement reached equilibrium once the capillary pressure became equal to the differential pressure between CO_2 and water. At this moment, the partial pressure of each phase reached the designed value. CO_2 saturation was obtained by measuring the volume of replaced water.

5) The stress in axis II was increased to a stable loading of 25 MPa, and the true triaxial test was then initiated after the loading was stabilized. The constant strain-rate loading was set to 1.0×10^{-5} s^{-1}.

Experimental results
Mechanical behavior of fluid-saturated sandstone under true triaxial conditions

Figure 2 shows the true triaxial test results for dry rocks and rocks containing N_2, CO_2, H_2O, and CO_2-H_2O biphase flow.

As seen, both gas and water showed weakening effects on the strength of the sandstone in the order of $H_2O > CO_2 > N_2$. Under the experimental conditions, the peak stresses of the dry sandstone, and N_2-, CO_2-, and H_2O-containing sandstone were 105.24 MPa, 96.57 MPa, 91.59 MPa, and 73.77 MPa, respectively, and their linear elastic moduli were 11.68 GPa, 10.90 GPa, 9.93 GPa and 8.88 GPa, respectively. In addition,

the dry sandstone had obvious brittle failure features. The H_2O-containing sandstone exhibited a significant strain softening phenomenon in the late rock failure stage, and the CO_2- and N_2-containing sandstones were mainly subject to brittle failure. In all, the pore gases reduced the brittleness of dry sandstone and increased its plastic deformation. The supercritical CO_2 had more significant effects than N_2.

The triaxial mechanical tests with the two-phase flow indicated that the peak stress of the sandstone under the action of CO_2 (10 MPa)-H_2O (8.5 MPa) two-phase flow was 84.388 MPa, higher than that of the H_2O-containing sandstone and lower than that of the CO_2-containing sandstone. The sandstone showed obvious brittle features under the action of the two-phase flow, indicating that CO_2 had more significant effects on the final brittle mechanical behavior of sandstone than H_2O. The elastic modulus in the elastic linear region of the two-phase flow coupled sandstone was 9.064 GPa, slightly higher than that of H_2O-containing sandstone but significantly lower than that of CO_2-bearing sandstone, indicating that the water affected the elastic modulus more significantly than CO_2 did.

Failure modes of fluid-saturated sandstone under true triaxial conditions

First, an SEM (scanning electron microscope) was used to characterize the microstructure information of failed samples. The test results are shown in Figure 3. To comparatively investigate the microstructure characteristics of sandstone with different fluids under true triaxial compression, the initial micromorphology of the original sandstone sample, not subject to stress damage and fluid effects, was obtained by SEM, as shown in Fig. 3(a). The initial micromorphology characteristics of mineral grains included random arrangement and good cementation; the bonds of grains were surface-to-surface contacts and point-to-surface contacts; surface-to-surface contact was predominant, and many pre-existing flaws, such as pores, microcracks, and voids, were easily observed. However, hardly any macrocracks were found in this sample.

As shown in Fig. 3(b), the shear surface of the dry failed specimen was relatively flat, the remaining mineral grains and clay remained relatively intact, and mineral grains were well bonded together by clay; no mesocrack appeared. Apparent cracks formed, but the
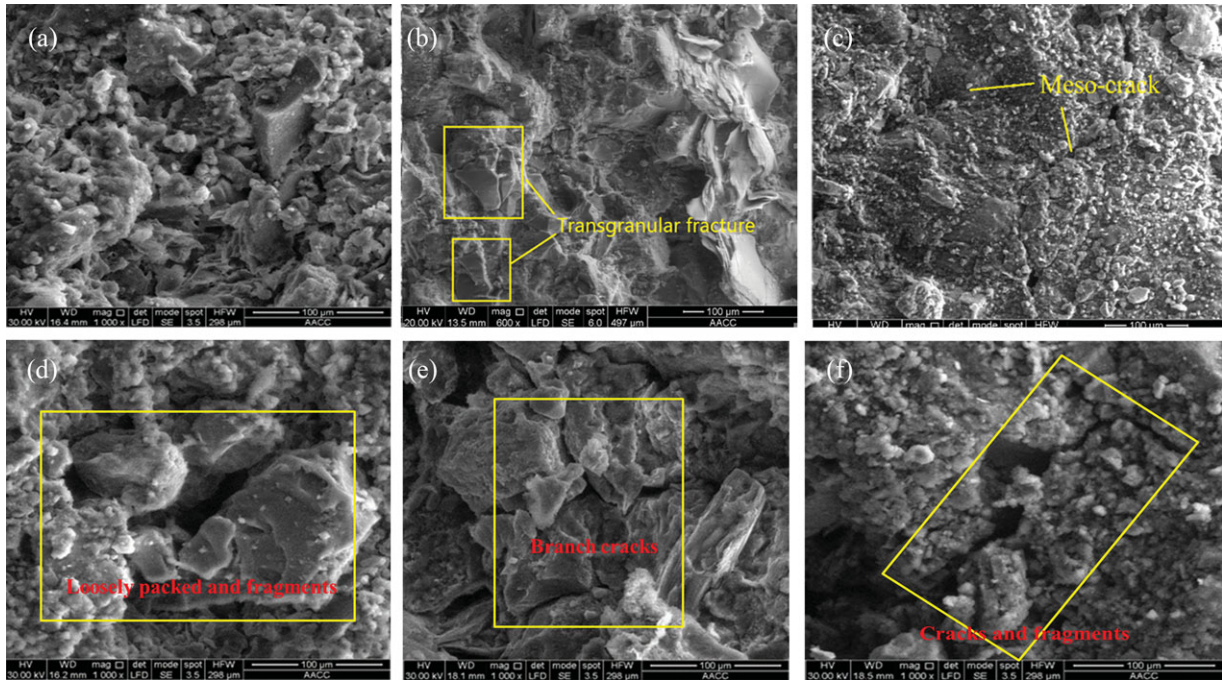
Figure 3. Scanning Electron Microscope of Microstructure of Sandstone under Different Pore Fluids: (a) initial micro-morphology of the original sandstone sample; (b) micro-morphology of dry failed specimen; (c) micro-morphology of failed sample under the action of H_2O; (d) initial micro-morphology of failed sample under the action of CO_2; (e) initial micro-morphology of failed sample under the action of N_2; (f) initial micro-morphology of failed sample under the action of CO_2-water biphase flow.

rest of the specimen was still well cemented by clay, and no clay came off from the shear surface. Figure 3(c) shows the micro-structure of the failed sample under the action of H_2O. We could observe mesocracks perpendicular to the shear plane, and the shear plane was flatter compared with the surface of the dry sample; no dimples appeared. Some particles peeled off from the shear surface and cementation; gathered into a bundle, they attached to the shear plane. In contrast, the microscopic structure of the sandstone under gas conditions was clearly different. SEM images of failed samples under the action of CO_2 and N_2 are presented in Figs 3(d) and 3(e), respectively. First, due to gas splitting, there were many small branch cracks within the sandstone. Meanwhile, grains were loosely packed, and a few fragments attached to the shear plane. Figure 3(f) shows SEM images of the failed sample under the action of CO_2-water biphase flow. It was clear that mesocracks perpendicular to the shear plane were observed. In addition, some particles also peeled from the shear surface and remained looser than in the other samples. Micro-voids were nucleated, propagated, and coalesced, and intergranular cracks appeared around grains. Because of the effects of

different pore fluids on the microscopic fracture structure of sandstone, there were clearly various failure modes of sandstone under the action of dissimilar pore fluids (CO_2/N_2/H_2O/CO_2-H_2O). We obtained several types of typical fracture propagation and failure modes. Due to the action of different pore fluids, the color of the rock changed under the action of the pore fluid. The specific results are shown in Fig. 4.

As shown in Fig. 4, dry sandstone and water-bearing sandstone often failed in the form of a single fracture surface damage. Compared with water, the differences of N_2 or CO_2 for crack extension of sandstone were more apparent. Under the action of N_2 or CO_2, outside the main fracture surface, another crack was derived in the main branch; cracks in the rock formed an 'X'. The results show that the CO_2-containing sandstone was characterized by multiple section rupture. At the same time, there were many crisscross small branch cracks near the main fracture, and branches of the main fractures of CO_2-containing sandstone were characterized by multiple section rupture. Under the condition of CO_2-H_2O biphase flow, the form of rock crack damage was the same as the crack propagation form under the action of N_2 or CO_2 gas, as shown in

Figure 4. Typical crack extension and failure modes of fluid-saturated sandstones: (a) injected CO_2; (b) injected N_2; (c) injected H_2O; (d) near CO_2 injection side under CO_2-H_2O biphase conditions; (e) near H_2O injection side under CO_2-H_2O biphase conditions; (f) dry.

Fig. 4. However, the difference was that, in the side near the ceramic plate, the cracks had certain differences compared to cracks under the action of carbon dioxide; small branch cracks close to the ceramic plate side decreased significantly. The non-uniformity of two-phase fluid, which was caused by the experimental method, more easily led to rupture of the interface.

Analysis and discussion

Effect of fluids on strength and micro-mechanical mechanisms of sandstone

It is well known that hydrous conditions strongly influence the mechanical behaviors of porous rocks.

Fluids act through two main mechanisms, namely, hydro-mechanical coupling and their chemical effects.[15] Effective stress is often used to quantitatively describe the variation of the strength of porous media. According to the principle of effective stress, sandstone should have the same strength under the same experimental conditions. However, under the same confining pressure, the strength of the dry sandstone was different, indicating that the effects of pore fluid on rock strength followed the order of $H_2O > CO_2 > N_2$.

To further confirm the different effects of pore fluids on rock strength, the mechanical experiments were conducted with the CO_2-H_2O biphase condition. Capillary forces could be generated under the condition of CO_2-H_2O biphase flow. Under partially
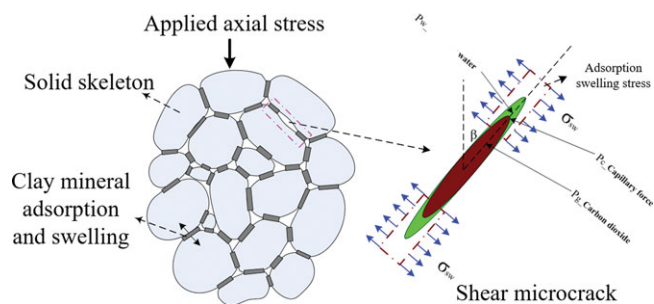
Figure 5. Illustration of the micro micro-mechanics mechanical mechanisms in porous rock.

saturated conditions, the poromechanical coupling was related to the development of capillary forces. Capillary forces, which increased the confining pressure of sandstone, hardened porous rocks. According to the monitoring results, the water saturation was 0.79 after the system was fully equilibrated. According to the effective stress model reported in the literature,[32] the effective confining pressure of two-phase flow coupled sandstone was 10.33 MPa. Theoretically, the strength of the CO_2-H_2O two-phase coupled rocks should be greater than those obtained with single phase fluids. However, the experimental strength of the sandstone under the action of 10 MPa CO_2 and 8.5 MPa H_2O was 84.388 MPa, higher than that of the H_2O-containing sandstone and lower than that of the CO_2-containing sandstone. These observations further suggest that the properties of the contained fluid exhibited significant effects on the rock strength.

In fact, various processes, such as ion exchange, physical adsorption, chemical adsorption, chemical dissolution and precipitation, and so on, can occur between the pore fluid and the mineral particle surfaces.[33–38] Therefore, in this paper, all tests were completed in 12 h to ensure that the changes in rock mechanical properties were attributed mainly to physical and chemical adsorption of N_2/CO_2/H_2O. Montmorillonite (MMT) interacting with CO_2 can result in changes of basal spacing and generate additional swelling stress, which has been verified by experimental methods.[39] Rock is usually formed by multiple cemented mineral particles. One part of them are detrital minerals that mainly bear the load, such as quartz; the other part are clay minerals such as montmorillonite that play a role in cementation and form microscopic pores and cracks between mineral particles, as shown in Fig. 5. Previous studies found that as a result of the deviatoric stress, tension cracks

and compressional shear cracks appeared inside rocks.[40–43] When the principal fracture propagated forward at its front ends, several groups of microcracks first occurred, either isolated from one another or forming fork-shapes, then connected to one another, forming macroscopic fractures and closing some microcracks around it.

In general, pores in cement minerals are more developed. When the pore fluid is injected into rock, the fluid permeates or diffuses into pores or microcracks in rock. Meanwhile, the interaction between cement minerals and fluid occurs, thereby changing their physicochemical properties. In this study, only the adsorption of these cement minerals was considered. After they adsorbed pore fluid, the lattice spacing of mineral particles was increased, resulting in expansive deformation. The magnitude of deformation depended not only upon the physicochemical surface energy[44,45] but also upon the nature of the pore fluid. When the biphase fluid was present in rock, interfacial tension formed between rock pores and fluid, resulting in the formation of additional matrix suction. Figure 6(a) is a schematic drawing of the analysis of force in the microscale when the biphase-fluid acted on the rock. Under the biphase-fluid action, tensile microcracks and shear microcracks were produced in the rock. The presence of pore fluid accelerated the expansion and propagation of microcracks (discussed in the next section), thereby weakening the strength of rock.

On the other hand, the pore fluid injected in the rock interacted with the surface lattices of the clay minerals, which reduced the surface energy of the clay minerals and increased lattice layer spacing. The additional swelling stress formed between the mineral particles further decreased the effective stress, which lowered the strength of the rocks. The sandstone minerals selected in the present study had the absorption abilities in the order of MMT>illite. MMT and illite have the strongest water absorption abilities, followed by CO_2 and N_2. Therefore, under the same conditions, the strengths of rocks are in the order of N_2-containing rocks>CO_2-containing rocks>H_2O-containing rocks.

Microcracking mechanism of fluid-containing sandstone

Previous studies focused on the micro- or macroscopic cracking modes of rocks subject to an applied load.[46–49] Griffith suggested that the formation of macroscopic
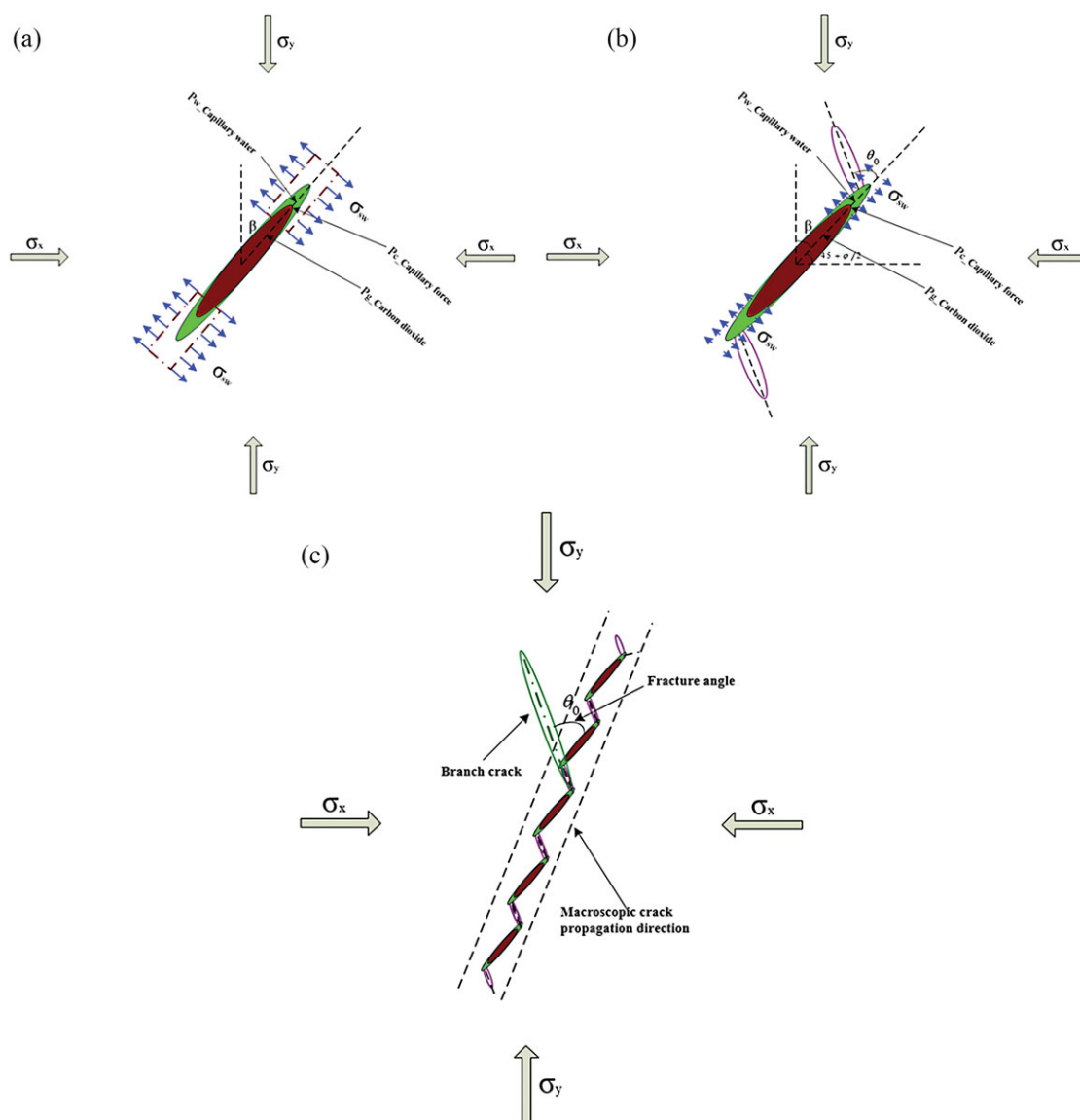
Figure 6. Micro - crack propagation schematic diagram under compressive-shear stress conditions: (a) schematic drawing of force analysis for compressional shear microcrack in rock core acted upon by biphase fluids; (b) schematic drawing of the direction angle and the fracture angle of the preferentially growing microcrack in the rock core; (c) schematic drawing of the formation of macroscopic cracks from micro- and mesoscopic cracks.

cracks in solids originated from their internal microcracks. It was found that the macroscopic fracture of rocks was closely related to its internal microstructures and microdefects. Experiments using scanning electron microscopy[40] on the relationship between microcracks and macroscopic fractures revealed two main failure patterns of rocks under the applied load: shear fracture and tension fracture. In the failure patterns of rock under applied deviatoric stress, the compressional shear failure pattern is dominant.[48]

Therefore, this article focuses on analyzing the effect of the pore-fluid injection on the cracks of the rock subject to compressional shear stress. Figure 6 shows a schematic drawing of its force analysis.

From Fig. 6(a), it is clear that the normal stress and shear stress produced by applied loading on the wall surface of a microcrack are:

$$\left. \begin{array}{l} \sigma_n = \sigma_y(\sin\beta)^2 + \sigma_x(\cos\beta)^2 \\ \tau_n = (\sigma_y - \sigma_x) \cdot \sin\beta \cdot \cos\beta \end{array} \right\} \quad (1)$$

 |

where β is the crack angle as shown in Fig. 6(a); σ_x and σ_y are the principal stresses in the X and Y directions, respectively; σ_n is the normal compressive stress of the crack; and τ_n is the shear stress of the crack.

The effective normal stress produced on the wall is:

$$\sigma_n^e = \sigma_n - P_g + X_a \cdot (P_g - P_w) - \sigma_{sw}$$
$$= \sigma_y(\sin \beta)^2 + \sigma_x(\cos \beta)^2$$
$$- P_g + X_a \cdot (P_g - P_w) - \sigma_{sw} \quad (2)$$

where σ_n^e is the equivalent normal compressive stress of the crack; P_g is the pressure of carbon dioxide; P_w is the pressure of water; X_a is the effective stress coefficient with water saturation; and σ_{sw} is the adsorption expansion stress due to the adsorption of clay minerals.

Assuming that the friction coefficient of the wall surface of the microcrack is u_f, the friction resistance produced by the normal stress is:

$$f = u_f \cdot \sigma_n^e = u_f \cdot (\sigma_y(\sin \beta)^2 + \sigma_x(\cos \beta)^2$$
$$- P_g + X_a \cdot (P_g - P_w) - \sigma_{sw}) \quad (3)$$

where f is friction on the crack surface.

The effective shear stress induced on the wall surface of the shear microcrack is:

$$\tau_n^e = \tau_n - f \quad (4)$$

where τ_n^e is the effective shear stress.

From fracture mechanics, a compressional shear crack is described as:

$$K_I = 0, K_{II} = \tau_n^e \cdot \sqrt{\pi \cdot a}, K_{III} = 0 \quad (5)$$

where K_I, K_{II}, and K_{III} are the stress intensity factors of the three typical cracks, and a is the length of the crack.

According to Shi and Madenci,[50] the stress energy density factor S of the Type II compressional shear crack derived from the stress energy density theory is:

$$S = \frac{(\tau_n^e)^2 \cdot a}{16\mu}[(k+1)(1 - \cos \theta)$$
$$+ (1 + \cos \theta)(3 \cos \theta - 1)] \quad (6)$$

From Eqn (6), the crack angle θ_0 and the minimum stress energy density factor S_{min} are found to be:

$$\theta_0 = -\arccos\left(\frac{k-1}{6}\right),$$

$$S\big|_{\theta=\theta_0} = S_{min} = \frac{(\tau_n^e)^2 \cdot a}{16\mu} \frac{[14k - k^2 - 1]}{12} = S_c \quad (7)$$

where μ is the shear modulus of the material, θ is the crack angle of the microcrack (deviating from the crack direction); $k = 3 - 4\nu$ (in the plane strain assumption); and $k = (3 - \nu)/(1 + \nu)$ (in the plane stress assumption).

Thus, the critical expansive shear stress is found as

$$\tau_n^c = \sqrt{\frac{192\mu \cdot S_c}{a \cdot (14k - k^2 - 1)}} \quad (8)$$

$$S_c = \frac{K_{IIC}^2}{12\pi \mu}(2 - 2v - v^2) \quad (9)$$

where S_c is a parameter describing the fracture roughness of materials (it is a constant for some material); K_{IIC} is the fracture roughness of a material subject to pure shear, in which case it can be measured; and v is Poisson's ratio.

From the theory of energy relief, the rate of crack expansion is given as follows:

$$K_{IIC} = \sqrt{E \cdot R_c} = \sqrt{E \cdot 2\gamma} \quad (10)$$

where E is the elastic modulus of the material, R_c is the critical resistance to crack expansion, and γ is the surface energy of the material per area.

From Eqns (1) to (9), the critical peak stress, i.e., axial loading σ_n^e, of rocks under different surrounding pressures can be obtained, where K_{IIC} can be measured through the pure-shear experimental test. For sandstone, its interior actually contains a large number of microscale cracks. The expansion and propagation of microcracks in the standard rock samples under applied compressional shear stress mainly depends on the effective shear stress. When it reaches its critical fracture toughness, microcracks start to crack. Assuming that inside the rock, a large quantity of microcracks are distributed at random angles, the expansion of microcracks in the range of 0–90 degrees can be analyzed as follows. According to Mohr's principle, taking the friction effect on the fracture surface into consideration, the microcrack has the maximum shear stress in the direction of $\beta = 90 - (45 + \varphi/2)$, and the microcrack expands first, as shown in Fig. 6(b).

From Eqn (7), the fracture angle at which the microcrack expands mainly depends upon Poisson's

Table 3. Tested and calculated results of mechanical parameters of sandstone containing 5 types of pore fluids under true triaxial compression.

Pore fluid	Peak stress σ/MPa	Elastic modulus E/GPa	Poisson's ratio μ
Dry	105.24	11.68	0.24
N_2	96.57	10.90	0.30
CO_2	91.59	9.93	0.34
CO_2-H_2O	84.39	9.06	0.35
H_2O	73.77	8.88	0.37

ratio v for sandstone. The Poisson's ratio of sandstone has a greater effect on the fracture angle. According to the stress-strain curves of sandstone with different pore fluids, the Poisson's ratios of dry, N_2-bearing, CO_2-bearing, CO_2-H_2O-bearing, and H_2O-bearing sandstone are 0.24, 0.30, 0.34, 0.35, and 0.37, respectively, as shown in Table 3.

Further, the macroscopic cracks of sandstone are formed by the expansion and run-through of a large number of micro- and mesocracks, as shown in Fig. 6(c). From Eqns (2)–(5), it is also clear that for compressional shear cracks, the presence of pore fluids increases the stress intensity factor at the crack tip, thus accelerating the extension of cracks. In addition, the greater the fluid pressure, the more significant this effect is, which further induces the formation of branch cracks. In this study, the Poisson's ratio of CO_2-bearing sandstone is 0.338, and the fracture angle θ_0 (the macroscopic crack deflection angle was obtained by direct measurement) is approximately 80.05° as calculated using Eqn (7), which is roughly consistent with the experimental results. Meanwhile, the adsorption of pore fluid reduces the surface energy of mineral particles, thereby lowering the fracture toughness of the rock and further leading to the observation that the branch cracks formed due to the injection of CO_2 into sandstone were more obvious than those due to the injection of N_2 under the same conditions. Clearly, the thermodynamic state of a fluid has evident effects on the extension of microcracks and the production of branch cracks.

Because of the different physical and chemical properties of the pore fluids, the effects of the pore fluids on the mechanical behavior of rocks were significantly different. Cracks in the rock acted upon by applied loads rapidly expanded, and the volume of the rock quickly increased, so that it was too late for these cracks to exchange their mass and energy. Thus, at this time, the fluid satisfied the condition of adiabatic

expansion for doing work. According to the assumption, the propagation of fluid in cracks can be considered as an isentropic expansion process. In its expansion process, the crack fluid does work on the crack walls and reduces its internal energy, density, pressure, and temperature, while the decreasing magnitudes of its state parameters are determined by its properties. For a compressible fluid, the change in pressure caused by the change per unit volume is significantly lower than that for a fluid that is hard to compress (e.g. water). Further, under the same conditions, the work done by a gas is greater than that done by a liquid.

According to the basic laws of thermodynamics, the relationships of pressure, temperature, and volume of an ideal gas in its isentropic process are as follows:

$$\frac{T_2}{T_1} = \left(\frac{P_2}{P_1}\right)^{(k-1)/k} = \left(\frac{V_1}{V_2}\right)^{k-1} \tag{11}$$

where T is the temperature of an ideal gas; P is the pressure; and k = C_p/C_v, where C_p is the isobaric heat capacity, and C_v is the isometric heat capacity.

From Eqn (11), the variations in temperature, pressure, and volume of an ideal gas in its isentropic expansion process given different initial states can be found. The pressure decrease of supercritical CO_2 or N_2 under the conditions of the same crack temperature and pressure in its isentropic expansion process is smaller; thus, its ability to do work during its expanding volume is greater than that of H_2O. According to the physical data of CO_2, N_2, and H_2O obtained from the chemical kinetics network database of the National Institute of Standards and Technology (NIST) in the United States, their entropic values at an initial pressure of 10 MPa and a temperature of 311 K are 1.3205 kJ/kg * K, 5.4593 kJ/kg * K, and 0.53988 kJ/kg * K, respectively; and the corresponding density values are 669.38 kg/m³, 107.11 kg/m³, and

 |

Table 4. Changes in parameters of crack fluids during the expansion of cracks.

	Ini. Fracture			Ext. Fracture					
	P_1/MPa	V_1/m³	T_1/k	P_2/MPa	V_2/m³	T_2/k	Ini. Density (kg/m³)	Int. Energy (kJ/kg)	Work (kJ)
CO_2	10	1	311	7.82	1.02	304.53	669.38	0.7	468.7
N_2	10	1	311	9.25	1.02	303.63	107.11	4.5	481.5
H_2O	10	1	311	0.1	1.02	310.77	997.33	0.02	19.95

997.33 kg/m³, respectively. Supposing that the volume of a microcrack increased by 0.02 times during the continuous expansion, the changes in pressure, density, internal energy, and temperature can be obtained when the volume expands up to 1.02 times its initial volume. Table 4 gives the calculated results.

At an initial pressure of 10 MPa and temperature of 311 K, after the isentropic expansion, the ratio of work done by CO_2, N_2 and H_2O was 23.5:24.1:1, and the ratio of their pressures was 7.82:9.25:0.1. Remaining higher CO_2, N_2 and H_2O pressures were conducive to the further expansion of cracks, until their pressures decreased below the critical expansion resistance. According to the experimental measurement results, the differences in effects of the three different pore fluids on sandstone cracking patterns were significant. The injection of CO_2 into sandstone formed an X-type principal fracture, around which many branch cracks were distributed; the injection of N_2 into sandstone also formed an X-type principal fracture but induced fewer fine branch cracks; the effect of water on sandstone cracking patterns was relatively much smaller, showing no significant difference compared to dry sandstone. In addition, at 10 MPa, the abilities of CO_2 and N_2 to do work were comparable, which is also the major reason that under the same experimental conditions, the crack distribution forms on the cracking surface of sandstone induced by the two types of crack fluids were similar. Compared with the ability of CO_2 to do work, the N_2-induced branch cracks should be more obvious, but in fact, just the opposite occurred. Analysts found that this result may be related to the adsorption of CO_2 on sandstone mineral compositions, and the adsorption of CO_2 leads to the reduction of the bonding effect on the surface of solid particles in the sandstone. Thus, with their comparable capacities to do work, CO_2 more easily cracks sandstone, forming more obvious branch cracks. Figure 7 shows the curves of P-V and T-V relationships of the three injected working media in their isentropic expansion processes.

As shown in Fig. 7, in the experiment, the crack propagated from its initial state, Point A, to Point B. Compared with H_2O and N_2, the P-V curve of CO_2 had an obvious turning point, indicating that near the turning point (the supercritical point), the pressure-drop rate of the supercritical CO_2 in its expansion process was much faster than that of the gaseous CO_2. Temperature and pressure were more sensitive to changes in volume. In this experiment, CO_2 in cracks was in the supercritical state. Although the expansion process of N_2 was similar to that of CO_2, the P-V curve of N_2 was smoother. Under the same conditions, the abilities of CO_2 and N_2 to do work toward the wall of cracks were comparable. However, for H_2O, due to its lower compression factor, its pressure-drop in the expansion process decreased rapidly from 10 MPa to 0.10 MPa; the temperature was relatively stable (fluctuation less than 1 k), and its ability to do work was only approximately 4% of those for CO_2 and N_2.

Clearly, the thermodynamic properties (pressure, temperature, and expansion for the capacity to do work) of the three working media, i.e., crack fluids, and their adsorption characteristics, jointly determine the extent of their impacts on the expansion of microcracks and pores inside the sandstone. The former influences the morphology of the principal fracture surface of the sandstone, while the latter affects the morphology of the expansion of branch cracks. Therefore, this experiment shows that cracks and porous fluids have important impacts on the formation of the fracture network. In the study of the development of cracks in a porous medium impacted by multiphase fluids, we are usually concerned with only the pressure of the crack fluid and analyze the extending length of cracks through the effective stress. However, this method has some discrepancies with reality, considering neither the thermodynamic properties of crack fluids including transient flow, heat exchange, phase change and others nor the absorption-weakening of pore fluids, resulting
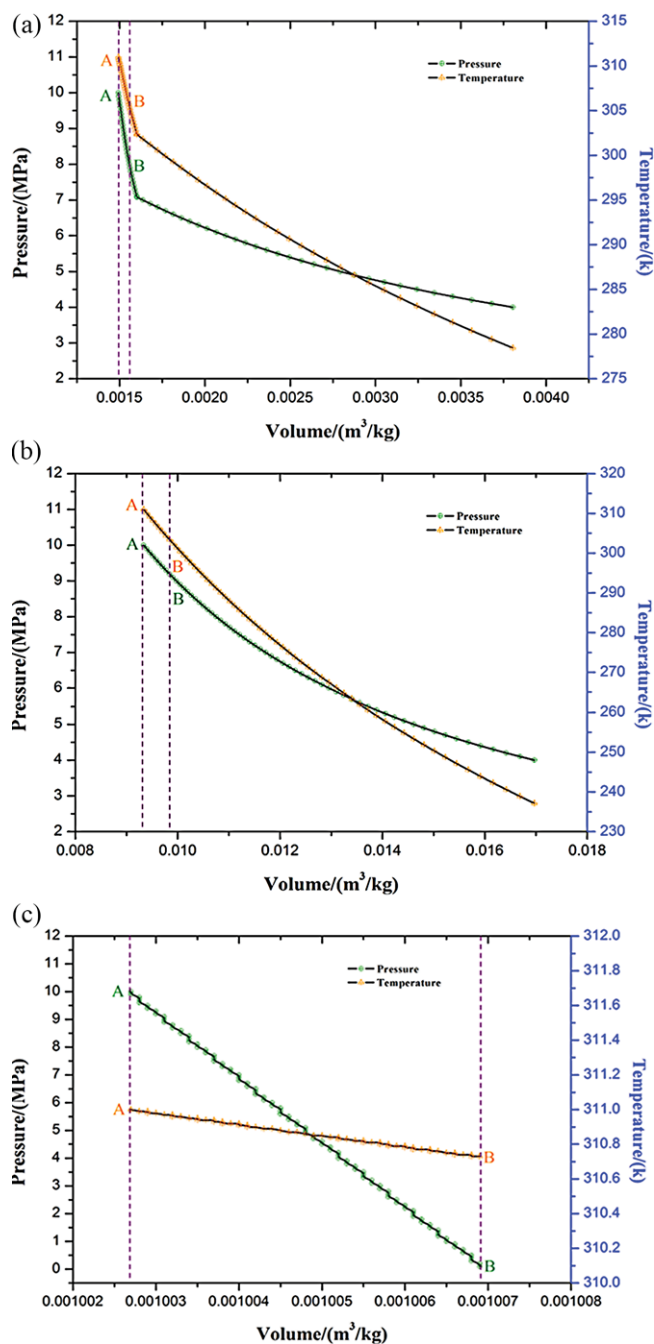
Figure 7. Curves of P-V and T-V relationships for three types of injected working media in their isentropic expansion processes: (a) injected CO_2; (b) injected N_2; (c) injected H_2O.

in the fact that the traditional method cannot explain many characteristic experimental phenomena.

Our study on the micro- and mesoscopic interaction mechanisms among pores fluids, crack fluids, and mineral particles in the sandstone showed that the

study of fluid-solid interactions in the sandstone should start mainly with the following aspects:

- Sandstone contains a large number of pores and microcracks; thus, fluid injected into sandstone also forms crack fluid and pore fluid, which exhibit different effects on rock mechanical properties. The impacts of pore fluid on rock mechanical properties and deformation can be explored using traditional effective stress principles and percolation theory, but the impacts of crack fluids on rock mechanical properties can be explored only with the consideration of the flow-for-heat-exchange characteristics and thermodynamic properties of crack fluids.

- The physical and chemical interactions occurring between pore fluids and rock minerals in the sandstone change the lattice spacing of rock minerals and their interactive forces, further affecting the macroscopic parameters of the rock such as the elastic modulus, cohesion, and internal friction angle, which in essence means changing the micro- and mesoscopic mechanical acting mechanisms between mineral particles and the solid surface energy. Therefore, studies on rock strength criteria, crack propagation and the damage evolution mechanism must fully consider the micro- and mesoscopic physical and chemical effects between the pore fluids and rock mineral interfaces.

- Acted upon by external loading, microcracks or pores satisfying the cracking conditions start to crack and expand, and pore fluids and crack fluids work together to promote the propagation and expansion of microcracks in the rock. The thermodynamic properties of crack fluids determine the morphology of a rock's principal fracture surface, while the adsorption properties of pore fluids affect the expansion morphology of branch cracks. Thus, it is necessary to simultaneously consider the status and role of biphase pore fluids in the study of rock damage and deformation.

The coupling mechanical behaviors induced by the injection of fluid into deep strata are very complex and significantly affected by temperature, formation stress, rock types and structure, and fluid types and phases, and they have complicated disastrous mechanisms, dynamic coupling, and multiple impacting factors. Our future study will focus on the effects of temperature, rock types (sedimentary rock, igneous rocks, etc.), fluid

phase changes, and crack morphology on the coupling mechanical behavior to reveal the key geomechanical and Earth system science issues related to the injection of different types of geothermal reservoir fluids into deep strata.

Conclusions

Pore fluids can differently affect the mechanical properties of a reservoir sandstone formed by the cementation of a variety of minerals, especially those containing clay minerals, in the order of $H_2O > CO_2 > N_2$. Compared with dry sandstone, the strengths of H_2O-, CO_2- and N_2-saturated sandstone decrease 29.89%, 12.97%, and 8.24%, respectively, under the same conditions and confining pressure. The tests with CO_2-H_2O two-phase flow indicate that CO_2 affects the mechanical behaviors of the sandstone more significantly after reaching the stress peak than H_2O and mainly causes brittle failure, which is unlike H_2O that mainly causes plastic deformation. The elastic modulus of the two-phase flow coupled rock is 9.064 GPa, greater than that of H_2O-containing sandstone and less than that of supercritical CO_2-containing sandstone, indicating that H_2O has more significant effects on the elastic modulus of rocks than supercritical CO_2. Supercritical CO_2 has high density, low viscosity, and easy diffusion and phase transition; thus, it affects the mechanical behaviors of sandstone differently from H_2O.

Sandstone contains large numbers of pores and microcracks, so fluid injected into rocks forms pore fluids and crack fluids inside them, which have clearly different effects on rock deformation and strength. The pore fluids mainly interact with internal mineral particles to alter the physical properties of mineral particle surfaces and reduce the interaction forces between mineral particles, thus affecting the macroscopic mechanical parameters of the rock. These effects can be better and quantitatively described using the traditional effective stress model and the strength softening model. By contrast, the crack fluid flow in the expansion process of cracks can be considered as an adiabatic isentropic expansion process. Between the crack fluids and the crack walls exists direct physical action; the heat- and mass-transferring characteristics of crack fluids directly determine the magnitudes of fluid action and the amount of work done on the crack walls during the extension of cracks, thus affecting the length of crack propagation. In the isentropic

expansion process at an initial pressure of 10 MPa and temperature of 311 K, the ratio of work done by CO_2, N_2 and H_2O was 23.5:24.1:1, and the pressure ratio was 7.82:9.25:0.1. The thermodynamic properties of the three working media determine the degrees of their impacts on the expansion of cracks inside sandstone. Compared with H_2O, injecting N_2 or CO_2 into sandstone was more prone to double shear failure, leading to the formation of many branch cracks around the principal fracture surface. This effect of CO_2 was more obvious. Acted upon by the external loading, the microcracks or pores satisfying the cracking conditions would start to crack and expand; both pore fluids and crack fluids work together to accelerate the expansion and extension of microcracks in sandstone. The thermodynamic properties of crack fluids determine the primary fracture surface morphology of the rock, and the adsorption characteristics of pore fluids affect the expansion patterns of branch cracks. Thus, it is necessary to simultaneously consider the states and effects of fluids in the biphase pore fluids. Based on fracture mechanics and thermodynamics, a mathematical and physical model for the mechanical expansion of rock microcracks subject to fluid can be established.

The true triaxial mechanical test system constructed in the present work for the two-phase flow-coupled rocks can accurately simulate the stresses and pore fluids in deep reservoirs. Our design provides a good experimental foundation for further studying the true triaxial mechanical properties of CO_2 geosequestration in reservoir rocks. The experimental evidence presented in this paper showed that the type, phase, and thermodynamic properties of the fluid have very significant impacts on the strength and cracking patterns of rock. Future study will focus on the effects of temperature, rock types (sedimentary rock, igneous rocks, etc.), changes in fluid phase, and crack morphology on the coupling mechanical behavior to clarify the key geomechanical and Earth system science issues related to the injection of different types of geothermal reservoir fluids into deep strata.

References

1. Holloway S and Savage D, The potential for aquifer disposal of carbon dioxide in the UK. *Energy Convers Manage* **34**(9–11):925–932 (1993).

2. Rigg A, Allison G, Bradshaw J, Ennis KJ, Gibson PC and Hillis RR, The search for sites for geological sequestration of CO_2 in Australia: a progress report on Geodisc. *Appea J* **41**(7):11–25 (2001).

3. Sminchak J, Gupta N, Byrer C and Bergman P, Issues related to seismic activity induced by the injection of CO_2 in deep saline aquifers. *J Energy Environ Res* **2**(1):32–46 (2002).

4. Rutqvist J, The geomechanics of CO_2 storage in deep sedimentary formations. *Geotech Geol Eng* **30**(3):525–551 (2012).

5. Keith FE, Zapponeb A, Kraftb T, Deichmannb N and Moiac F, A survey of the induced seismic responses to fluid injection in geothermal and CO_2 reservoirs in Europe. *Geothermics* **41**:30–50 (2012).

6. Ranjith PG and Perera, MS, A new triaxial apparatus to study the mechanical and fluid flow aspects of carbon dioxide sequestration in geological formations. *Fuel* **90**:2751–2759 (2011).

7. Viete DR and Ranjith PG, The effect of CO_2 on the geomechanical and permeability behavior of brown coal: implications for coal seam CO_2 sequestration. *Int J Coal Geol* **66**(3):204–216 (2006).

8. Gentzis T, Deisman N and Chalaturnyk RJ Geomechanical properties and permeability of coals from the Foothills and Mountain regions of western Canada. *Int J Coal Geol* **69**(3):153–164 (2007).

9. Crews JB and Cooper CA, Transient pore pressure response to confining stress excursions in Berea sandstone flooded with an aqueous solution of CO_2. *Water Resour Res* **50**:4775–4786 (2014).

10. Younane NA, SonK H and MinhH T, Mechanical characterization of small shale samples subjected to fluid exposure using the inclined direct shear testing device. *Int J Rock Mech Mining Sci* **47**:355–367 (2010).

11. Chenevert M and Pernot V, Control of shale swelling pressures using inhibitive water-base muds. *Proceedings of SPE Annual Technical Conference and Exhibition*, 27–30 September, New Orleans, LO, USA (1998).

12. Wan RG, Achari G, Schacter R, Joshi RC and McLellan PJ, Time-dependent effect of drilling fluids on Fernie shales. *J Can Pet Technol* **37**(5):47–51 (1998).

13. Huang H, Azar JJ and Hale AH, Numerical simulation and experimental studies of shale interaction with water-base drilling fluid. *Proceedings of IADC/SPE Asia Pacific Drilling Conference*, 7–9 September, Jakarta, Indonesia, paper IADC/SPE 47796 (1998).

14. Chenevert ME and Amanullah M, Shale preservation and testing techniques for borehole-stability studies. *SPE Drilling Completion* **16**(3):146–149 (2001).

15. Grgic D and Giraud A, The influence of different fluids on the static fatigue of a porous rock: Poro-mechanical coupling versus chemical effects. *Mech Mat* **71**:34–51 (2014).

16. Rostom F, Royne A, Dysthe DK and Renard F, Effect of fluid salinity on subcritical crack propagation in calcite. *Tectonophysics* **583**:68–75 (2012).

17. Philip MB, Vinciguerra S, Philip GM and Young RP, Spatio-temporal evolution of volcano seismicity: A laboratory study. *Earth Planet Sci Lett* **297**:315–323 (2010).

18. Schoenball M, Muller TM, Muller BIR and Heidbach O, Fluid-induced microseismicity in pre-stressed rock masses. *Geophys J Int* **180**:813–819 (2010).

19. Li Q, Wu Z, Lei X and Takashi S, Experimental and numerical study on the fracture of rocks during injection of CO_2-saturated water. *Environ Geol* **51**(7):1157–1164 (2007).

20. Niezgoda T, Miedzinska D, Malek E, Kedzierski P and Slawinski G, Study on carbon dioxide thermodynamic behavior for the purpose of shale rock fracturing. *Bull Polish Acad Sci Tech Sci* **61**(3):605–611 (2013).

21. Liu T, Cao P and Lin H, Damage and fracture evolution of hydraulic fracturing in compression shear rock cracks. *Theoretical and Applied Fracture Mechanics* **74**:55–63 (2014).

22. Yoshitaka N, Kazuya M, Tetsuro Y, Naoki H and Katsuhiko K, Effects of humidity and temperature on subcritical crack growth in sandstone. *International Journal of Solids and Structures* **48**:1130–1140 (2011).

23. Nara Y and Kaneko K, Sub-critical crack growth in anisotropic rock. *Int J Rock Mech Min Sci* **43**:437–453 (2006).

24. Nara Y, Hiroyoshi N, Yoneda T and Kaneko K, Effect of temperature and relative humidity on subcritical crack growth in igneous rock. *Int J Rock Mech Min Sci* **47**:640–646 (2010).

25. Nara Y, Morimoto K, Yoneda T, Hiroyoshi N and Kaneko K, Effects of humidity and temperature on subcritical crack growth in sandstone. *Int J Solids Struct* **48**:1130–1140 (2011).

26. Liteanu E, Spiers CJ and De Bresser JHP, The influence of water and supercritical CO_2 on the failure behavior of chalk. *Tectonophysics* **599**:157–169 (2013).

27. Liu M, Bai B and Li X, Experimental studies on the short-term effect of CO_2 on the tensile failure of sandstone. *Energy Procedia* **63**:3357–3363 (2014).

28. Bachu S and Adams JJ, Sequestration of CO_2 in geological media in response to climate change: capacity of deep saline aquifers to sequester CO_2 in solution. *Energy Convers Manage* **48**(31):51–75 (2003).

29. Urata Y, Hok S, Fukuyama E and Madariaga R, The effect of thermal pressurization on dynamic fault branching. *Geophys J Int* **196**(2):1–10 (2013).

30. Lu M and Luke DC, The transient behavior of CO_2 flow with phase transition in injection wells during geological storage: Application to a case study. *J Petrol Sci Eng* **124**:7–18 (2014).

31. GB/T 23561.2 (2009) Methods for determining the physical and mechanical properties of coal and rock-Part 2: Methods for determining the true density of coal and rock.

32. Papamichos E, Brignoli M and Santarelli FJ, An experimental and theoretical study of a partially saturated collapsible rock. *Mech Cohes Friction Mat* **2**(3):251–278 (1997).

33. Le Guen Y, Renard F, Hellmann R, Brosse E, Collombet M, Tisserand D and Gratier JP, Enhanced deformation of limestone and sandstone in the presence of high pressure CO_2 fluids. *J Geophys Res* **112**(B5):622–634 (2007).

34. Madland MV, Finsnes A, Alkafadgi A, Risnes R and Austad T, The influence of CO_2 gas and carbonate water on the mechanical stability of chalk. *J Petrol Sci Eng* **51**:149–168 (2006).

 |

35. Vialle S and Vanorio T, Laboratory measurements of elastic properties of carbon-ate rocks during injection of reactive CO_2-saturated water. *Geophys Res Lett* **38**:L01302 (2011).

36. Croizé D, Bjørlykke K, Jahren J and Renard F, Experimental mechanical and chemical compaction of carbonate sand. *J Geophys Res* **115**(B11):581–638 (2010).

37. Schutjens PM, Experimental compaction of quartz sand at low effective stress and temperature conditions. *Journal of the Geological Society of London* **148**:527–539 (1991).

38. Renard F, Park A, Ortoleva P and Gratier JP, An integrated model for transitional pressure solution in sandstone. *Tectonophysics* **312**:97–115 (1999).

39. Romanov VN, Evidence of irreversible CO_2 intercalation in montmorillonite. *Int J Greenh Gas Control* **14**:220–226 (2013).

40. Zhong J, Liu S, Ma Y, Yin C, Liu C, Li Z, Macro-fracture mode and micro-fracture mechanism of shale. *Petrol Explor Dev* **42**(2):242–250 (2015).

41. Liu J, Wang E, Song D, Wang S and Niu Y, Effect of rock strength on failure mode and mechanical behavior of composite samples. *Arab J Geosci* **8**:4527–4539 (2015).

42. Lawson H, Weakley A and Miller A, Dynamic failure in coal seams: Implications of coal composition for bump susceptibility. *Int J Mining Sci Technol* **26**:3–8 (2016).

43. Oraec K, Oraec N, Goodarzi A and Khajehpour P, Effect of discontinuities characteristics on coal mine stability and sustainability: A rock fall prediction approach. *International Journal of Mining Science and Technology* **26**:65–70 (2016).

44. Tone K, Kamori M and Shibasaki Y, Effect of the Surface Potential on the Cation Exchange Capacity of Kaolin Minerals. *Clay Sci* **10**(4):327–335 (1998).

45. Jarvie DM, Hill KJ, Time E, Ruble R and Pollastro M, Unconventional shale-gas systems: The Mississippian Barnett shale of north central Texas as one model for thermogenic shale-gas assessment. *AAPG Bull* **91**(4):475–499 (2007).

46. Walsh JB, The effect of cracks on the compressibility of rocks. *J Geophys Res* **20**(2):381–384 (1965).

47. Niandou H, Shao JF, Henny JP and Fourmaintraux D, Laboratory investigation of the behavior of Tournemire shale. *Int J Rock Mech Mining Sci* **34**(4):3–16 (1997).

48. Liang C, Wu S and Li X, Research on micro-meso characteristics of grantie fracture under uniaxial compression at low and intermediate strain rates. *Chinese J Rock Mech Eng* **34**(1):2977–2985 (2015).

49. Ma C, Li T, Cheng G and Cheng Z, A micro particle model for hard brittle rock and the effect of unloading rock burst. *Chinese J Rock Mech Eng* **34**(2):217–227 (2015).

50. Shi GC and Madenci E, Crack growth resistance characterized by the strain energy density function. *Eng Fract Mech* **18**(6):1159–1171 (1983).

Shaobin Hu

Shaobin Hu is a lecturer in Tunnel and Underground Engineering Institute, College of Civil and Transportation Engineering, HoHai University, JiangSu, NanJing, China, who received his PhD from China University of Mining & Technology (Xuzhou) in 2015 and complete his postdoctoral Research in Institute of Rock and Soil Mechanics, Chinese Academy of Sciences. His main research interests include Carbon dioxide nanocomposite blasting and fracturing.

Bing Bai

Bing Bai, associate professor, Institute of Rock and Soil Mechanics, CAS, China. He has, since 2003, been engaged in the studies of geomechanics relating to CO_2 storage and deep underground energy recovery. Representative achievements include the design methodology of CO_2 redline wellhead injection pressure of China Shenhua CCS pilot project. He is also the secretory of Theme 6, U.S-China Clean Energy Research Center on Advanced Coal Technology Consortium (CERC-ACTC 1.0).

Xiaochun Li

Xiaochun Li is a senior research scientist and research group leader at the State Key Laboratory of Geomechanics and Geotechnical Engineering in Wuhan, Institute of Rock and Soil Mechanics, Chinese Academy of Sciences. He is one of the pioneer scientists to introduce CCS into China since 2004. Li has engaged in research and development of CO_2 geological sequestration technology, and has made a series of vital achievements in interactions of rock failure and see page, site selection, and mechanical stability.